Intent Prediction in Human-Human Interactions*

Murchana Baruah† Bonny Banerjee†‡ Atulya K. Nagar§

Abstract

The human ability to infer others' intent is innate and crucial to development. Machines ought to acquire this ability for seamless interaction with humans. We propose an agent model for predicting the intent of actors in human-human interactions. This requires *simultaneous generation and recognition of an interaction* at any time, for which end-to-end models are scarce. The proposed agent actively samples its environment via a sequence of glimpses. At each sampling instant, the model infers the observation class and completes the partially observed body motion. It learns the sequence of body locations to sample by jointly minimizing the classification and generation errors. The model is evaluated on videos of two-skeleton interactions under two settings: (first person) one skeleton is the modeled agent and the other skeleton's joint movements constitute its visual observation, and (third person) an audience is the modeled agent and the two interacting skeletons' joint movements constitute its visual observation. Three methods for implementing the attention mechanism are analyzed using benchmark datasets. One of them, where attention is driven by sensory prediction error, achieves the highest classification accuracy in both settings by sampling less than 50% of the skeleton joints, while also being the most efficient in terms of model size. This is the first known attention-based agent to learn end-to-end from two-person interactions for intent prediction, with high accuracy and efficiency.

Keywords: Agent, intent prediction, interaction recognition and generation, attention, perception, proprioception.

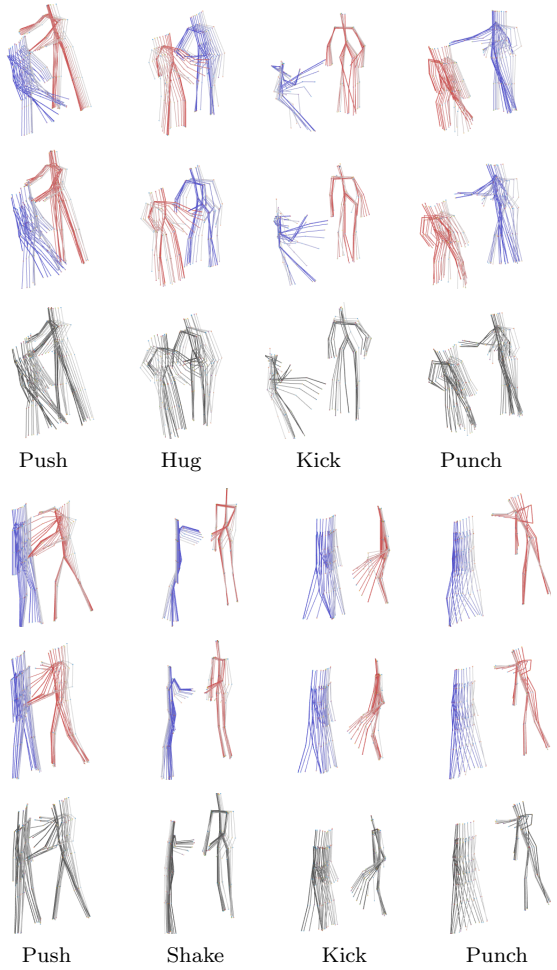

Figure 1: Rows 1–3 show the actual, generated first and third person videos respectively for four interactions from SBU Kinect Interaction dataset. Rows 4–6 show the same for four interactions from K3HI dataset. Recent frames are darker in shade than older frames. Best viewed in color.

1 INTRODUCTION

The ability to perceive others as intentional agents is innate and crucial to development [1]. Appropriate interpretation of others' intentions is the key to a successful interaction [2]. In AI, human intent prediction has been extensively studied in the context of different applications such as assistive robotics, human-robot interaction, video and robotic surveillance, and autonomous driving. *We refer to "intent prediction" as the problem of simultaneously inferring the action/interaction class and generating the involved persons' future body motions.*

*A version of this article will appear in IEEE Transactions on Human-Machine Systems as [**?**].

†Institute for Intelligent Systems, and Department of Electrical & Computer Engineering, University of Memphis, Memphis, TN 38152, USA. Email: MurchanaBaruah@gmail.com, BonnyBanerjee@yahoo.com.

‡Corresponding author.

§School of Mathematics, Computer Science and Engineering, Liverpool Hope University, Hope Park, Liverpool L16 9JD, UK. Email: nagara@hope.ac.uk.

We propose an attention-based agent model that learns to predict the intent of two-person interactions from 3D skeletal data. Forecasting interaction motions is a challenging problem as the model has to learn the spatiotemporal dependencies among the skeletal joints of the two persons. Training a model by minimizing generation and classification errors in conjunction may lead to more stability and less overfitting due to each error acting as a regularizer for the other [3].

Contributions. The proposed attention-based agent model actively predicts the intent of the persons in its environment, interacts with them in a closed perception-action loop, and is learned end-to-end. The novelties of this work are as follows:
(1) The action (attention) is modeled as proprioception in a multimodal setting. Reinforcement signal or utilities/values of states are not required in the model.
(2) At each sampling instant, the model simultaneously predicts the interaction class and the motion of both 3D skeletons. This happens for both first person (FP) and third person (TP) environments. Typically FP models, such as [4, 5], generate the motion of only one skeleton.
(3) Three methods for implementing action selection (or attention mechanism) are analyzed. Classification accuracy is comparable when sampling locations are determined from prediction error (without any weighting) or from learned weights (without involving prediction error); however, the latter is less efficient in terms of model size.
(4) In our model, classification and generation pathways share a subset of parameters, and hence depend on each other. However, highest generation accuracy does not necessarily lead to highest classification accuracy.
(5) The method, where attention is driven by sensory prediction error (without any weighting), achieves the highest classification accuracy in both FP and TP environments. It samples less than 50% of the skeleton joints from each frame on average, and is the most efficient in terms of model size.

The proposed agent model is the first of its kind to interact with and learn end-to-end from two-person interaction environments in FP and TP for intent prediction, with high accuracy and efficiency.

2 Related Work

A number of models have been reported for two-person interaction generation (e.g., [6–8]), reaction generation (e.g., [4, 5, 9, 10]), or two-person interaction recognition (e.g., [11–16]) using 3D skeletal data. The problem of interaction generation, i.e. generating the interaction sequence of both skeletons, is more challenging than the reaction generation problem where the goal is to generate the reaction sequence of one skeleton given the action sequence of another.

In these works, the environment is viewed from one of two perspectives: first person (FP) where one of the interacting persons is the observer while the other constitutes his environment (e.g., [4, 5, 10]), or third person (TP) where a person, such as an audience, is the observer and the two interacting persons constitute his environment (e.g., [7]).

Very few models perform both generation and recognition. In a model, generation and recognition can be performed either separately such as [9], or simultaneously such as [10] and our current work. We utilize a variational recurrent neural network (RNN)-based model to generate both interacting skeletons in both FP and TP, while [10] uses a generative adversarial network to generate only the reacting skeleton in FP. We are not aware of any model for simultaneous generation and recognition of two-person interactions.

Some of these models are attention-based. They utilize different attention mechanisms, such as temporal (e.g., [10, 14, 17–19]), spatiotemporal (e.g., [12, 20]), multimodal (e.g., [21, 22]), or multilayer (e.g., [13]). In most models, attention is implemented by strategically introducing additional learnable parameters. For example, a transformer-based attention mechanism is used in [9], and a sequence-to-sequence long short-term memory (LSTM)-based attention layer is used in [10], both of which introduce additional attention parameters learned during training. In our model, attention is computed directly from the generation error, which is why generation is necessary. There is no attention parameter in our model. Not only does our model yield the state-of-the-art recognition accuracy while being efficient, we show that introducing learnable attention parameters to weigh the generation error does not necessarily increase the accuracy on benchmark datasets.

3 Models and Methods

3.1 Preliminaries

Agent is anything that perceives its environment via sensors and acts upon the environment using actuators [23]. In this paper, the agent is simulated in software.
Perception is the mechanism that allows an agent to interpret the state of its external environment from sensory signals [24].
Proprioception is perception where the environment is the agent's own body. Proprioception allows an agent to internally perceive the state (location, motion, etc.) of its body [24].
Generative model. A generative model, p_{model}, maximizes the log-likelihood $\mathcal{L}(x;\theta)$ of the data, where θ is a set of parameters and x is a set of data points [25].
Evidence lower bound (ELBO). If z is a latent continuous random variable generating the data x, computing log-likelihood requires computing the integral of the marginal likelihood, $\int p_{model}(x,z)dz$, which

is intractable [26]. Variational inference involves optimization of an approximation of the intractable posterior by defining an evidence lower bound (ELBO) on the log-likelihood, $\mathcal{L}(x;\theta) \leq \log p_{model}(x;\theta)$.

Variational autoencoder (VAE) is a deep generative model that assumes the data consists of independent and identically distributed samples, and the prior, $p_\theta(z)$, is an isotropic Gaussian. VAE maximizes the ELBO given by [26], $\mathcal{L}(x;\theta) \leq \mathbb{E}_{q_\phi(z|x)}[\log p_\theta(x|z)] - D_{\mathrm{KL}}(q_\phi(z|x), p_\theta(z))$, where $q_\phi(z|x)$ is a recognition model, $p_\theta(x|z)$ is a generative model, $\mathbb{E}$ denotes expectation, and D_{KL} denotes Kullback-Leibler divergence.

Saliency is a property of each location in an agent's environment that regulates his attention. We consider multiple attention mechanisms, some of which are functions of the agent's prediction error while the others are not.

3.2 Problem Statement

Let $\mathbf{X} = \{\mathbf{X}^{(1)}, \mathbf{X}^{(2)}, \ldots, \mathbf{X}^{(n)}\}$ be a set of observable variables representing an environment in n modalities. The variable representing the i-th modality is a sequence: $\mathbf{X}^{(i)} = \langle X_1^{(i)}, X_2^{(i)}, \ldots, X_T^{(i)} \rangle$, where T is the sequence length. Let $\mathbf{x}_{\leq t} = \{\mathbf{x}_{\leq t}^{(1)}, \ldots, \mathbf{x}_{\leq t}^{(n)}\}$ be a partial observation of $\mathbf{X}$ such that $\mathbf{x}_{\leq t}^{(i)} = \langle x_1^{(i)}, \ldots, x_t^{(i)} \rangle$, $1 \leq t \leq T$. Let $\mathbf{y} = \langle y_1, \ldots, y_T \rangle$ where y_t represents the true class label at time t. We define the problem of *pattern completion* as generating $\mathbf{X}$ and $\mathbf{y}$ as accurately as possible from the partial observation $\mathbf{x}_{\leq t}$. At any time t, the objective is to maximize the joint likelihood of $\mathbf{X}$ and $\mathbf{y}$ given $\mathbf{x}_{\leq t}$ and a generative model p_θ with parameters θ, i.e., $\arg\max_\theta p_\theta(\mathbf{X}, \mathbf{y}|\mathbf{x}_{\leq t})$.

3.3 Agent Architecture

The proposed agent architecture comprises of five components: environment, observation, pattern completion and classification, action selection, and learning. See block diagrams in Fig. 2.

1. Environment. The environment is the source of time-varying data. We consider first and third person environments.

First person (FP): One of the two skeletons is modeled as the first person (a.k.a. *primary agent*). His body constitutes his internal environment while the *other skeleton* constitutes his external (visual) environment. Two modalities are used to model the primary agent (see Fig. 2a): (i) visual perception which captures the other skeleton's 3D joint coordinates, and (ii) body proprioception which captures his own (primary agent skeleton's) 3D joint coordinates.

Third person (TP): The agent is modeled as a third person (e.g., an audience). The two interacting skeletons constitute his external (visual) environment.

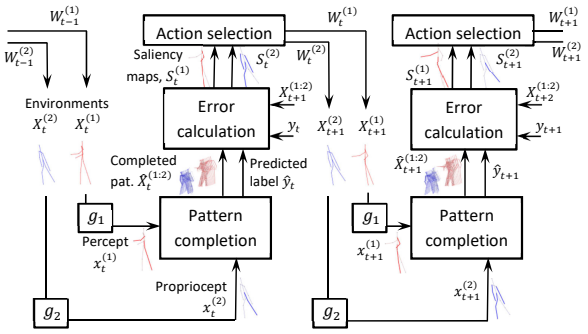

(a) First person (FP) perspective involving two modalities: visual perception (superscript 1) and body proprioception (superscript 2). Without loss of generality, the blue skeleton is considered as the primary agent (first person) while the red skeleton constitutes its visual observations. Best viewed in color.

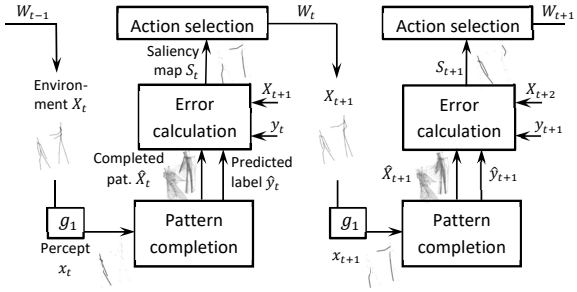

(b) Third person (TP) perspective involving only one modality: visual perception. Hence, superscript indicating the modality is not shown.

Figure 2: Block diagrams of our attention-based agent applied to two-person interaction classification via generation.

Only the visual perception modality is used to model the third person, which captures both skeletons' 3D joint coordinates (see Fig. 2b).

2. Observation. The agent interacts with its environment via a sequence of eye and body movements. The observations, sampled from the environment at each time instant, are in two modalities: perceptual and proprioceptive. In the benchmark skeleton datasets, there is no information regarding the appearance of joints (shape, color, texture) but only their location. The appearance constitutes visual perception ('what') while location constitutes visual proprioception ('where'). There is only one visual modality in this model, referred to as visual perception (could also be called visual proprioception), in both FP and TP (Fig. 2).

3. Pattern completion. A multimodal variational recurrent neural network (MVRNN) for variable length sequences is used to complete the patterns for all modalities. Recognition and generation are the two processes involved in the operation of an MVRNN.

Recognition (Encoder). The recognition model $q_\phi(z_t|\mathbf{x}_{\leq t}, z_{<t})$ is a probabilistic encoder [26]. It

produces a Gaussian distribution over the possible values of the code z_t from which the observations $\mathbf{x}_{\leq t}$ could have been generated.

The MVRNN consists of two RNNs, each with one layer of LSTM units. Each RNN generates the parameters for the approximate posterior distribution and the conditional prior distribution for each modality, as in [27].

The distribution parameters from all modalities are combined using product of experts (PoE), as in [28], to generate the joint distribution parameters for the conditional prior $p_\theta(z_t|\mathbf{x}_{<t}, z_{<t})$, and the approximate posterior $q_\phi(z_t|\mathbf{x}_{\leq t}, z_{<t})$. The recognition model is formulated as:

$$[\mu_{0,t}^{(i)}\ \sigma_{0,t}^{(i)}] = \varphi_\tau^{prior}(h_{t-1}^{(i)}), \quad [\mu_{z,t}^{(i)}\ \sigma_{z,t}^{(i)}] = \varphi_\tau^{enc}(x_t^{(i)}, h_{t-1}^{(i)})$$
$$z_t \sim \mathcal{N}(\mu_{0,t}, \sigma_{0,t}), \quad z_t|x_t \sim \mathcal{N}(\mu_{z,t}, \sigma_{z,t})$$
$$\sigma_{0,t}^2 = \Big(\sum_i {\sigma_{0,t}^{(i)}}^{-2}\Big)^{-1}, \quad \sigma_{z,t}^2 = \Big(\sum_i {\sigma_{z,t}^{(i)}}^{-2}\Big)^{-1}$$
$$\mu_{0,t} = \Big(\sum_i \mu_{0,t}^{(i)} {\sigma_{0,t}^{(i)}}^{-2}\Big)\sigma_{0,t}^2, \quad \mu_{z,t} = \Big(\sum_i \mu_{z,t}^{(i)} {\sigma_{z,t}^{(i)}}^{-2}\Big)\sigma_{z,t}^2$$

where $h_{t-1}^{(i)}$ is the hidden state at $t-1$ for modality i, φ_τ^{prior} generates the mean as a linear function of its input, φ_τ^{enc} generates the logarithm of standard deviation as a non-linear function of its input, φ_τ^{prior} accepts the hidden state as input, and φ_τ^{enc} accepts the hidden state and the current observation as input. See Lines 2–10 of Algorithm 2 in Suppl.

Here, ϕ^{prior} generates the mean as a linear function of its input, ϕ^{enc} generates the logarithm of standard deviation as a non-linear function of its input, ϕ^{prior} accepts the hidden state as input, and ϕ^{enc} accepts the hidden state and the current observation as input.

Generation (Decoder). The generative model, $p_\theta(X_t^{(1)}, X_t^{(2)}, y_t|\mathbf{x}_{<t}, z_{\leq t})$, generates the perceptual and proprioceptive data and the class label from the latent variables, z_t, at each time step.

Each RNN in the MVRNN generates the distribution parameters of the sensory data for a modality. The sensory data is sampled from this distribution. We assume the perceptual and proprioceptive distributions to be multivariate Gaussian as the skeletal joints are real-valued. We assume the class label distribution to be multivariate Bernoulli.

The generative model is formulated as:

$$h_t^{(i)} = RNN_\theta(z_t, x_t^{(i)}, h_{t-1}^{(i)}), \quad [\mu_{x^{(i)},t}^{(i)}\ \sigma_{x^{(i)},t}^{(i)}] = \varphi_\tau^{dec}(z_t, h_t^{(i)}).$$

For generation, $X_{t+1}^{(i)}|z_t \sim \mathcal{N}(\mu_{x^{(i)},t}^{(i)}, \sigma_{x^{(i)},t}^{(i)})$. For classification, $\hat{y}_t = f(h_t^{(n+1)}, z_t)$, where $h_t^{(n+1)} = f_\theta(z_t, \mathbf{x}_t, h_t^{(1:n)}, h_{t-1}^{(n+1)})$. Here RNN_θ represents an LSTM unit, φ_τ^{dec} is the same function as φ_τ^{enc}, and f is a softmax function. See Lines 11–15 of Algorithm 2 in Suppl.

The pattern, $\mathbf{X}$, is completed at each time using an iterative method. At any time t, the model predicts $\hat{\mathbf{x}}_{t+1}$ given the observations $\mathbf{x}_{k:t}$ $(1 \leq k < t)$, then predicts $\hat{\mathbf{x}}_{t+2}$ given $\{\mathbf{x}_{k+1:t}, \hat{\mathbf{x}}_{t+1}\}$, then predicts $\hat{\mathbf{x}}_{t+3}$ given $\{\mathbf{x}_{k+2:t}, \hat{\mathbf{x}}_{t+1:t+2}\}$, and so on till $\hat{\mathbf{x}}_T$ is predicted. This method allows a fixed and finite model to predict a variable or infinite length sequence. Since only the next instant is predicted at any iteration, the model can be size efficient.

4. Action selection. In the proposed model, action selection is to decide the weight (attention) given to each location in the environment in order to sample the current observation. At any time t, a saliency map $S_t^{(i)}$ is computed for modality i from which the action is determined. The saliency map assigns a salience score $S_{t,l}^{(i)}$ to each location l. There are 15 locations corresponding to the 15 skeleton joints: Head (J1), Neck (J2), Torso (J3), Left Shoulder (J4), Left Elbow (J5), Left Hand (J6), Right Shoulder (J7), Right Elbow (J8), Right Hand (J9), Left Hip (J10), Left knee (J11), Left foot (J12), Right Hip (J13), Right knee (J14), Right foot (J15). We compute the weights in three ways as follows.

Weights are determined by thresholding the prediction error (*pe*). The threshold is statistically estimated on the fly and is not predetermined.

$$S_t^{(i)} = \|X_{t+1}^{(i)} - \hat{X}_{t+1}^{(i)}\|_1\ , \quad S_{t,r}^{(i)} = \tfrac{1}{|r|}\textstyle\sum_{l\in r} S_{t,l}^{(i)}$$
$$W_{t,l}^{(i)} = \begin{cases} 1, & \text{if } S_{t,l}^{(i)} \geq \frac{1}{n_r}\sum_{i=1}^{n_r} S_{t,r}^{(i)} \\ 0, & \text{otherwise} \end{cases}$$
$$x_{t+1}^{(i)} = W_t^{(i)} X_{t+1}^{(i)} + (1 - W_t^{(i)})\hat{X}_{t+1}^{(i)} \tag{1}$$

where $X_{t+1}^{(i)}, \hat{X}_{t+1}^{(i)}$ are the true and predicted data (skeleton joint coordinates) respectively, $\|.\|_1$ denotes L_1 norm, $|.|$ denotes the cardinality of a set, $n_r = 5$ is the number of regions in the skeleton (J1-J3, J4-J6, J7-J9, J10-J12, J13-J15) (see Fig. 4 in Suppl.), and $S_{t,r}^{(i)}$ is the mean saliency over the joints in region r.

At any time, at least one region will be salient. Our experiments show that variable number of salient regions at each time step is more effective. Fixing the number of salient regions to a constant value occasionally leads to selection of regions with low saliency or overlooking regions with high saliency. In our model, the salient joints are sampled while the observation from non-salient joints at time $t+1$ is the predicted observation from t.

Weights are learned as coefficients of the prediction error (*lwpe*).

$$S_t^{(i)} = W_a(X_{t+1}^{(i)} - \hat{X}_{t+1}^{(i)})$$
$$W_t^{(i)} = \sigma(S_t^{(i)})\ , \quad x_{t+1}^{(i)} = W_t^{(i)} X_{t+1}^{(i)} \tag{2}$$

Weights are learned as coefficients of hidden states (*lw*).

$$S_t^{(i)} = W_a h_t^{(i)},\ W_t^{(i)} = \sigma(S_t^{(i)}),\ x_{t+1}^{(i)} = W_t^{(i)} X_{t+1}^{(i)} \tag{3}$$

In Eqs. 2 and 3, W_a is the weight matrix to be learned. Eqs. 1, 2, 3 implement the functions g_1, g_2 in Fig. 2 (also see Lines 7, 8 of Algorithm 1 in Suppl.).

6. Learning. The objective is to maximize Eq. 4. Its derivation is shown in Suppl.

$$\mathbb{E}_{q_\phi(z_{\leq T}|\mathbf{x}_{\leq T})}\Big[\sum_{t=1}^{T}\sum_{i=1}^{2}\lambda_i \log p_\theta(X_t^{(i)}|z_{\leq t}, \mathbf{x}_{<t}) + \lambda_3 \log p_\theta(y|z_{\leq T}, \mathbf{x}_{<T})\Big] - \beta\sum_{t=1}^{T} D_{KL}\big(q_\phi(z_t|\mathbf{x}_{\leq t}, z_{<t}), p_\theta(z_t|\mathbf{x}_{<t}, z_{<t})\big) \quad (4)$$

where λ_1, λ_2, λ_3, β are the weights balancing the terms. Here $i = 1, 2$ for FP, and $i = 1$ for TP.

4 Experimental Results

4.1 Datasets

Our model is evaluated on two datasets:

SBU Kinect Interaction Dataset [29] consists of videos of eight two-person interactions: departing, approaching, pushing, hugging, kicking, exchanging object, punching, and shaking hands. The data, recorded from 7 participants, contains 21 sets. Each set consists of a unique pair of participants performing the eight interactions. The dataset has around 300 interaction videos, ranging from 9 to 46 frames. We divide the dataset into five distinct train-test splits, as in [29].

Kinect-based 3D Human Interaction (K3HI) Dataset [30] consists of videos of eight two-person interactions: departing, approaching, kicking, pointing, punching, pushing, shaking hands, and exchanging object. The data is recorded from 15 volunteers. Each pair of participants performs the eight interactions. The dataset has around 320 interaction videos, ranging from 20 to 104 frames. We divide the dataset into four distinct train-test splits, as in [30].

4.2 Experimental setup

We use a recurrent hidden layer of 256 units and a latent layer of 20 variables for each modality in the MVRNN. These parameters are estimated empirically. T is variable as interaction videos are of different lengths. Stochastic gradient descent, with a minibatch size of 100, is used to train the model. Adam optimization with a learning rate of 0.001 and default hyperparameters ($\beta_1 = 0.9$, $\beta_2 = 0.999$) are used. The objective function parameters (β, λ_1, λ_2) are fixed to 1, and $\lambda_3 = \alpha = 50$. To avoid overfitting, we use a dropout probability of 0.8 at the hidden layer for generation, and 0.1 at the hidden layer for classification. All hyperparameters, except the defaults, are estimated from the training set by cross-validation.

The skeletal data in SBU is normalized. No further preprocessing is done. We standardize the skeletal data in K3HI. Training models on handcrafted features defeats the purpose of learning. Hence we operate on raw skeletal data.

Model variations: For each environment, FP and TP, we experiment with the three action selection methods (ref. "Action selection" in Section 3.3): *pe*, *lwpe*, and *lw*.

Ablation study—Baseline, *bs* (w/o attention): Due to lack of end-to-end models that simultaneously generate and classify two-person interactions from 3D skeletal data, our model's performance is evaluated using an ablation study which we refer to as the baseline, *bs*. The goal is to understand the utility of attention in our model. For that, we create a baseline model (*bs*) by eliminating attention (Lines 7–8 in Algorithm 1 in Suppl.) from our model and presenting the true skeletal data as input. The MVRNN is modified such that the observation is sampled from all the joints (i.e., weight distribution is uniform over all joints) from both the skeletons at any time. For a fair comparison, the number of layers and the number of neurons in each layer are the same for all variants, {*bs*, *pe*, *lwpe*, *lw*}, in FP and TP.

Evaluation metrics: We evaluate the generation using results using average frame distance (AFD), as in [4]: $\frac{1}{T-1}\sum_t \|X_t^{(i)} - \hat{X}_t^{(i)}\|^2$, where $X_t^{(i)}$ and $\hat{X}_t^{(i)}$ are the true and predicted skeletal joint coordinates respectively at time t for modality i and T is the sequence length. We evaluate the classification using accuracy, recall, precision and F-score.

4.3 Evaluation Results

4.3.1 Qualitative evaluation

Fig. 1 shows one time step ahead prediction of the two skeletons (perception and body proprioception) for four kinds of interactions from each dataset. These figures are shown for both FP and TP, using *pe* action selection method. The prediction over space and time looks quite realistic for all cases. Figs. 5, 6, 7, 8 in Suppl. show the visual and body proprioceptive pattern completion when 30%, 50% and 70% of the frames have been observed. Our model generates realistic predictions over space and time for all the cases. As expected, short-term predictions are more accurate than long-term predictions. Even in the long-term, there is continuity and the two predicted skeletons are well synchronized. Our model's predicted action/reaction at each time step complies with the actual interactions.

4.3.2 Evaluation for generation accuracy

The AFD from FP is lower than or comparable to TP in most cases (ref. Table 1). Observing the two skeletons as distinct modalities helps to learn a better latent representation, resulting in more accurate generation. FP models have more parameters than TP which also explains the lower AFD from FP.

For both datasets, *pe* yields the highest AFD, while *lwpe* and *lw* yield AFD very close to *bs* which is the lowest. At each frame, *pe* samples less than 50% of the skeleton joints on average (ref. Tables 6, 7 in Suppl.), *lwpe* and *lw* weigh all the joints, while *bs* observes the entire skeleton. The generation accuracy of all model variants, {*bs*, *pe*, *lwpe*, *lw*}, in both FP and TP is lower than that of our model in [8], which is similar to *pe* but for two-skeleton interaction generation only. In the current model, generation is not the primary goal but is necessary to calculate attention from generation error. Unlike some models, no bone length constraint is explicitly used in any of our models, including that in [8]. Our models learn the spatiotemporal relations between joint locations in each skeleton using the VRNN in each modality and between the two skeletons using the PoE, in an end-to-end manner.

Table 1: Generation accuracy (AFD) averaged over all train-test splits (mean, std. dev.). Lowest AFD among {*pe*, *lwpe*, *lw*} for each dataset is highlighted.

Action Selection	SBU dataset		K3HI dataset	
	FP	TP	FP	TP
bs	.045, .01	.059, .02	.027, .05	.036, .05
pe	.148, .04	.137, .04	.040, .04	.056, .04
lwpe	**.044, .01**	.073, .02	**.027, .05**	.037, .05
lw	.045, .01	.062, .02	.029, .05	.033, .05

4.3.3 Evaluation for classification accuracy

The classification accuracy for our FP models is higher than or comparable to our TP models. Also, the number of trainable parameters for FP model (∼1.66M) is higher than that of TP model (∼1.09M).

In all experiments, our top performing attention model yields an accuracy very close to but not higher than the baseline (*bs*). The goal of attention in our model is to foster efficiency, discussed in the next section. Also, our *bs*' accuracy is higher than the state-of-the-art on both datasets on raw skeleton. Among non-attentional interaction classification models, the state-of-the-art accuracy for SBU is 93.3% [31] from raw skeleton while our non-attentional *bs* yields 93.7%. The state-of-the-art accuracy for K3HI is 48.54% [32] from raw skeleton while our *bs* yields 87.5%.

FP: For SBU, *bs* yields the highest classification accuracy followed by *pe* and *lwpe*. For K3HI, *bs* yields the highest accuracy followed by *lw* and *pe*.

TP: For SBU, *bs* yields the highest classification accuracy followed by *lw* and *pe*. For K3HI, *bs* yields the highest accuracy followed by *pe* and *lwpe*. See Table 3.

Thus, for both datasets and in both FP and TP, *pe* is either the top performer or a close second, excluding *bs*. Given that *pe* performs the worst in generation, we conclude that, among the three action selection methods in our model, highest generation accuracy does not necessarily lead to highest classification accuracy even though the generation and classification pathways share a subset of parameters. Further, the top performing *pe* is more efficient than *lwpe* and *lw* in terms of model size (ref. Table 8 in Suppl.). Since implementation of attention does not introduce any learnable parameter, there is no improvement in accuracy in *pe* over *bs*.

Comparison to models that performed both classification and generation: As stated in Section 2, we are not aware of any model that performs generation and recognition of two-person interactions. To the best of our knowledge, only two models, [9] and [10], perform generation and recognition. However, both of them solve the problem of reaction generation, while our model solves the more challenging problem of interaction generation. In [9], classification accuracy is 80% and 46.4% for SBU and K3HI respectively, which are much lower than ours (ref. Table 3). In [10], classification accuracy is 79.2% for aggressive emotions (kick, push, punch) and 39.97% for neutral emotions (hug, shake hands, exchange objects) for SBU, which are much lower than ours (ref. Table 3). This is summarized in Table 2.

Table 2: Comparison of classification accuracy (%) between our model and existing models that performed both generation and recognition. Detailed results from our model are presented in Table 3. Note that in terms of sampling efficiency, *pe* (attention-based) is twice as efficient as *bs* (non-attentional).

Data	Interaction generation		Reaction generation	
	Our model (FP, *bs*)	Our model (FP, *pe*)	[9]	[10]
SBU	93.2	93.1	80.0	39.97–79.2
K3HI	87.5	85.9	46.4	–

4.3.4 Evaluation for efficiency

The purpose of attention in our model is to increase sampling efficiency, evaluated as the average (over all videos in each interaction class) of the proportion of skeleton joints sampled from each frame. There is not much variation in this average between the three action selection methods for both the datasets and for both FP and TP (ref. Tables 6, 7 in Suppl.). On average, for any interaction class, *pe* samples less than 50% of the joints in any frame. Our non-attentional *bs* yields slightly higher classification accuracy because it observes 100% of the

Table 3: Classification results averaged over all train-test splits (mean, std. dev.). Highest accuracy among {*pe*, *lwpe*, *lw*} for each dataset is highlighted.

Data	Env.	Action	Accuracy	Recall	Precision	F-score
SBU	FP	*bs*	93.2, 4.7	.934, .04	.931, .05	.928, .05
		pe	**93.1, 3.75**	.940, .03	.924, .04	.925, .03
		lwpe	93.1, 3.9	.939, .04	.929, .04	.929, .04
		lw	91.5, 6.0	.920, .05	.902, .07	.903, .07
	TP	*bs*	93.7, 6.1	.944, .05	.935, .05	.934, .06
		pe	92.5,5.5	.930, .05	.927, .05	.922, .05
		lwpe	91.3, 7.5	.915, .06	.907, .08	.906, .07
		lw	92.9, 5.8	.951, .03	.921, .05	.924, .05
K3HI	FP	*bs*	87.5, 7.1	.865, .08	.859, .08	.856, .08
		pe	85.9, 5.2	.854, .07	.838, .06	.839, .06
		lwpe	84.9, 3.5	.850, .05	.818, .03	.818, .03
		lw	**86.9, 4.3**	.865, .05	.852, .05	.853, .05
	TP	*bs*	83.0, 6.6	.827, .07	.816, .08	.813, .08
		pe	82.7, 7.3	.816, .08	.815, .08	.810, .08
		lwpe	82.1, 4.5	.809, .04	.800, .06	.796, .05
		lw	80.8, 6.3	.793, .07	.775, .08	.777, .08

joints in each frame, and hence is less efficient. Most works, including [9,10], do not report sampling efficiency or model size.

It is important that generation and recognition accuracies vary with the proportion of ground truth frames observed in the same way for our attention (*pe*, *lw*, *lwpe*) and non-attention (*bs*) models. Fig. 3 shows that, even though *pe* samples less than 50% of the joints in each frame, it does not need to observe more ground truth frames to reach the same accuracy as *bs*. During the first few sampling instants, both generation and classification accuracies improve exponentially. The accuracies saturate after a certain percentage of frames, which occurs faster for generation than classification.

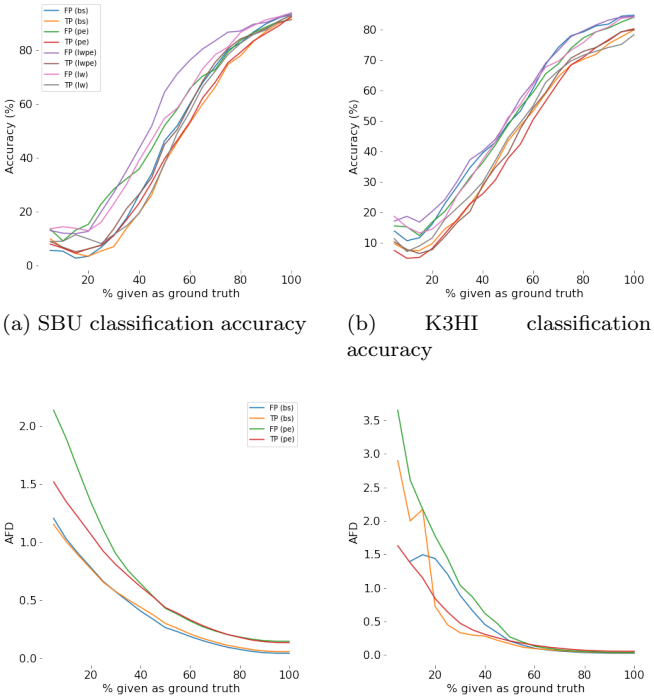

(a) SBU classification accuracy (b) K3HI classification accuracy

(c) SBU generation accuracy (d) K3HI generation accuracy

Figure 3: Generation and classification accuracy for different percentage of ground truth given as input for different environments and datasets.

5 Conclusions

A novel agent model is proposed that sequentially samples and interacts with its environment constituted of 3D skeletons. The agent operates as a closed-loop system involving perceptual ('what') and proprioceptive ('where') pathways which are learned end-to-end. At each instant, it samples the skeleton joints to jointly minimize its classification and generation errors in a greedy manner. Three sampling methods (or attention mechanisms) are analyzed of which one stands out for achieving high classification accuracy while being the most sample- and size-efficient. Experiments on intent prediction (interaction classification and body motion generation) using benchmark datasets reveal that the model yields state-of-the-art classification accuracy among those that operate on raw skeleton data. This is the first work to report a model's classification and generation accuracy on two-skeleton interaction videos. The superior accuracy and efficiency of our novel agent model is expected to inspire research on the design, analysis and experimentation with similar models.

References

[1] A. L. Woodward. Infants' grasp of others' intentions. *Curr. Dir. Psychol. Sci.*, 18(1):53–57, 2009.

[2] A. M. Wetherby and B. M. Prizant. The expression of communicative intent: Assessment guidelines. In *Semin. Speech Lang.*, volume 10, pages 77–91, 1989.

[3] D. L. Marino, K. Amarasinghe, and M. Manic. Simultaneous generation-classification using LSTM. In *IEEE Symp. Ser. Comput. Intell.*, pages 1–8, 2016.

[4] D. Huang and K. Kitani. Action-reaction: Forecasting the dynamics of human interaction. In *ECCV*, pages 489–504. Springer, 2014.

[5] E. Ng, D. Xiang, H. Joo, and K. Grauman. You2me: Inferring body pose in egocentric video via first and second person interactions. In *CVPR*, pages 9890–9900, 2020.

[6] J. N. Kundu et al. Cross-conditioned recurrent networks for long-term synthesis of inter-person

human motion interactions. In *WACV*, pages 2724–2733, 2020.

[7] T. Yao, M. Wang, B. Ni, H. Wei, and X. Yang. Multiple granularity group interaction prediction. In *CVPR*, pages 2246–2254, 2018.

[8] M. Baruah and B. Banerjee. A multimodal predictive agent model for human interaction generation. In *CVPR Workshops*, 2020.

[9] Baptiste Chopin, Hao Tang, Naima Otberdout, Mohamed Daoudi, and Nicu Sebe. Interaction transformer for human reaction generation. *arXiv preprint arXiv:2207.01685*, 2022.

[10] Q. Men, H. P. H. Shum, E. S. L. Ho, and H. Leung. GAN-based reactive motion synthesis with class-aware discriminators for human–human interaction. *Computers & Graphics*, 102:634–645, 2022.

[11] C. Li, Q. Zhong, D. Xie, and S. Pu. Co-occurrence feature learning from skeleton data for action recognition and detection with hierarchical aggregation. *arXiv:1804.06055*, 2018.

[12] S. Song, C. Lan, J. Xing, W. Zeng, and J. Liu. An end-to-end spatio-temporal attention model for human action recognition from skeleton data. In *AAAI*, pages 4263–4270, 2017.

[13] Z. Fan, X. Zhao, T. Lin, and H. Su. Attention-based multiview re-observation fusion network for skeletal action recognition. *IEEE Trans. Multimedia*, 21(2):363–374, 2018.

[14] F. Baradel, C. Wolf, and J. Mille. Pose-conditioned spatio-temporal attention for human action recognition. *arXiv:1703.10106*, 2017.

[15] Y. Qin, L. Mo, C. Li, and J. Luo. Skeleton-based action recognition by part-aware graph convolutional networks. *Vis. Comput.*, 36(3):621–631, 2020.

[16] M. Li and H. Leung. Multi-view depth-based pairwise feature learning for person-person interaction recognition. *Multimed. Tools Appl.*, 78(5):5731–5749, 2019.

[17] P. Vinayavekhin et al. Focusing on what is relevant: Time-series learning and understanding using attention. In *ICPR*, pages 2624–2629. IEEE, 2018.

[18] T. Fernando, S. Denman, S. Sridharan, and C. Fookes. Soft+ hardwired attention: An LSTM framework for human trajectory prediction and abnormal event detection. *Neural Netw.*, 108:466–478, 2018.

[19] J. Yu et al. A discriminative deep model with feature fusion and temporal attention for human action recognition. *IEEE Access*, 8:43243–43255, 2020.

[20] D. Varshneya and G. Srinivasaraghavan. Human trajectory prediction using spatially aware deep attention models. *arXiv:1705.09436*, 2017.

[21] Y. Hoshen. Vain: Attentional multi-agent predictive modeling. In *NIPS*, pages 2701–2711, 2017.

[22] A. Vemula, K. Muelling, and J. Oh. Social attention: Modeling attention in human crowds. In *ICRA*, pages 1–7. IEEE, 2018.

[23] S. Russell and P. Norvig. *Artificial Intelligence: A Modern Approach*. Prentice Hall, 4th edition, 2020.

[24] J. Han, G. Waddington, R. Adams, J. Anson, and Y. Liu. Assessing proprioception: A critical review of methods. *J. Sport Health Sci.*, 5(1):80–90, 2016.

[25] I. Goodfellow. NIPS 2016 tutorial: Generative adversarial networks. *arXiv:1701.00160*, 2016.

[26] D. Kingma and M. Welling. Auto-encoding variational Bayes. *arXiv:1312.6114*, 2013.

[27] J. Chung et al. A recurrent latent variable model for sequential data. In *NIPS*, pages 2980–2988, 2015.

[28] M. Wu and N. Goodman. Multimodal generative models for scalable weakly-supervised learning. In *NIPS*, pages 5575–5585, 2018.

[29] K. Yun, J. Honorio, D. Chattopadhyay, T. Berg, and D. Samaras. Two-person interaction detection using body-pose features and multiple instance learning. In *CVPR Workshops*, pages 28–35. IEEE, 2012.

[30] T. Hu, X. Zhu, W. Guo, and K. Su. Efficient interaction recognition through positive action representation. *Math. Probl. Eng.*, 2013, 2013.

[31] J. Liu, A. Shahroudy, D. Xu, A. C. Kot, and G. Wang. Skeleton-based action recognition using spatio-temporal LSTM network with trust gates. *IEEE Trans. Pattern Anal. Mach. Intell.*, 40(12):3007–3021, 2017.

[32] T. Hu, X. Zhu, S. Wang, and L. Duan. Human interaction recognition using spatial-temporal salient feature. *Multimed. Tools Appl.*, 78(20):28715–28735, 2019.

[33] D. P. Kingma, S. Mohamed, D. J. Rezende, and M. Welling. Semi-supervised learning with deep generative models. In *NIPS*, pages 3581–3589, 2014.

S Supplemental Material (Suppl.)

S.1 Loss function derivation

Here we derive the objective function in Eq. 4 from the objectives of multimodal VAE [28], variational RNN [27], and VAE for classification [33]. The generative and recognition models are factorized as:

$$p_\theta(\mathbf{X}_{\leq T}, y_{\leq T}, z_{\leq T}|\mathbf{x}_{\leq T}) = \prod_{t=1}^{T} p_\theta(\mathbf{X}_t, y_t|z_{\leq t}, \mathbf{x}_{<t}) p_\theta(z_t|\mathbf{x}_{<t}, z_{<t})$$

$$q_\phi(z_{\leq T}|\mathbf{x}_{\leq T}) = \prod_{t=1}^{T} q_\phi(z_t|\mathbf{x}_{\leq t}, z_{<t}).$$

The variational lower bound (ELBO) on the joint log-likelihood of the generated data, $\log p_\theta(\mathbf{X}_{\leq T}, y_{\leq T}|\mathbf{x}_{\leq T})$, is derived as:

$$\begin{aligned}
&\mathbb{E}_{q_\phi(z_{\leq T}|\mathbf{x}_{\leq T})}\Big[\log p_\theta(\mathbf{X}_{\leq T}, y_{\leq T}|\mathbf{x}_{\leq T}) \frac{q_\phi(z_{\leq T}|\mathbf{x}_{\leq T})}{q_\phi(z_{\leq T}|\mathbf{x}_{\leq T})}\Big] \\
&= \mathbb{E}_{q_\phi(z_{\leq T}|\mathbf{x}_{\leq T})}\Big[\log \frac{p_\theta(\mathbf{X}_{\leq T}, y_{\leq T}, z_{\leq T}|\mathbf{x}_{\leq T})}{p_\theta(z_{\leq T}|\mathbf{x}_{\leq T})} \frac{q_\phi(z_{\leq T}|\mathbf{x}_{\leq T})}{q_\phi(z_{\leq T}|\mathbf{x}_{\leq T})}\Big] \\
&= \mathbb{E}_{q_\phi(z_{\leq T}|\mathbf{x}_{\leq T})}\Big[\sum_{t=1}^{T} \log \frac{p_\theta(\mathbf{X}_t, y_t|z_{\leq t}, \mathbf{x}_{<t}) p_\theta(z_t|\mathbf{x}_{<t}, z_{<t})}{p_\theta(z_t|\mathbf{x}_{<t}, z_{<t})} \\
&\quad \frac{q_\phi(z_t|\mathbf{x}_{\leq t}, z_{<t})}{q_\phi(z_t|\mathbf{x}_{\leq t}, z_{<t})}\Big] \\
&= \mathbb{E}_{q_\phi(z_{\leq T}|\mathbf{x}_{\leq T})}\Big[\sum_{t=1}^{T} \Big[\log p_\theta(\mathbf{X}_t, y_t|z_{\leq t}, \mathbf{x}_{<t}) \\
&\quad - \log \frac{q_\phi(z_t|\mathbf{x}_{\leq t}, z_{<t})}{p_\theta(z_t|\mathbf{x}_{<t}, z_{<t})} + \log \frac{q_\phi(z_t|\mathbf{x}_{\leq t}, z_{<t})}{p_\theta(z_t|\mathbf{x}_{<t}, z_{<t})}\Big]\Big] \\
&\geq \mathbb{E}_{q_\phi(z_{\leq T}|\mathbf{x}_{\leq T})}\Big[\sum_{t=1}^{T} \log p_\theta(\mathbf{X}_t, y_t|z_{\leq t}, \mathbf{x}_{<t})\Big] \\
&\quad - \sum_{t=1}^{T} D_{KL}\big(q_\phi(z_t|\mathbf{x}_{\leq t}, z_{<t}), p_\theta(z_t|\mathbf{x}_{<t}, z_{<t})\big).
\end{aligned}$$

We assume, the modalities are conditionally independent given the common latent variables [28] and all observations till the current time. Therefore,

$$\log p_\theta(\mathbf{X}_t, y_t|z_{\leq t}, \mathbf{x}_{\leq t}) = \sum_{i=1}^{2} \log p_\theta(X_t^{(i)}|z_{\leq t}, \mathbf{x}_{<t}) + \log p_\theta(y_t|z_{\leq t}, \mathbf{x}_{<t}).$$

Thus,

$$\begin{aligned}
&\log p_\theta(\mathbf{X}_{\leq T}, y_{\leq T}|\mathbf{x}_{\leq T}) \\
&\geq \mathbb{E}_{q_\phi(z_{\leq T}|\mathbf{x}_{\leq T})}\Big[\sum_{t=1}^{T}\sum_{i=1}^{2} \log p_\theta(X_t^{(i)}|z_{\leq t}, \mathbf{x}_{<t}) \\
&\quad + \log p_\theta(y_t|z_{\leq t}, \mathbf{x}_{<t})\Big] \\
&\quad - \sum_{t=1}^{T} D_{KL}\big(q_\phi(z_t|\mathbf{x}_{\leq t}, z_{<t}), p_\theta(z_t|\mathbf{x}_{<t}, z_{<t})\big) \\
&\geq \mathbb{E}_{q_\phi(z_{\leq T}|\mathbf{x}_{\leq T})}\Big[\sum_{t=1}^{T}\sum_{i=1}^{2} \lambda_i \log p_\theta(X_t^{(i)}|z_{\leq t}, \mathbf{x}_{<t}) \\
&\quad + \lambda_3 \log p_\theta(y_t|z_{\leq t}, \mathbf{x}_{<t})\Big] \\
&\quad - \beta \sum_{t=1}^{T} D_{KL}\big(q_\phi(z_t|\mathbf{x}_{\leq t}, z_{<t}), p_\theta(z_t|\mathbf{x}_{<t}, z_{<t})\big)
\end{aligned}$$

where λ_1, λ_2, λ_3, β are the weights balancing the terms. Assuming the class label does not change over time, we simplify the above expression as:

$$\begin{aligned}
&\mathbb{E}_{q_\phi(z_{\leq T}|\mathbf{x}_{\leq T})}\Big[\sum_{t=1}^{T}\sum_{i=1}^{2} \lambda_i \log p_\theta(X_t^{(i)}|z_{\leq t}, \mathbf{x}_{<t}) \\
&\quad + \lambda_3 \log p_\theta(y|z_{\leq T}, \mathbf{x}_{<T})\Big] \\
&\quad - \beta \sum_{t=1}^{T} D_{KL}\big(q_\phi(z_t|\mathbf{x}_{\leq t}, z_{<t}), p_\theta(z_t|\mathbf{x}_{<t}, z_{<t})\big).
\end{aligned}$$

S.2 Pseudo code of algorithms

The five regions in the skeleton are shown in Fig. 4. The pseudo codes are shown in Algorithms 1, 2.

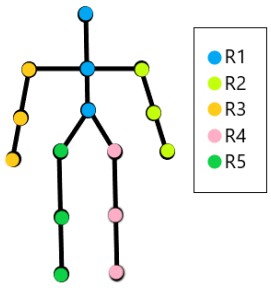

Figure 4: Different regions in the skeleton.

S.3 Experimental results

Details of our experimental results are provided here.

S.3.1 Performance evaluation

See Tables 4, 5, 6, 7.

Table 4: Generation accuracy (AFD) averaged over all train-test splits (mean, std. dev.) for **SBU Kinect Interaction dataset**. *bs*, *pe*, *lwpe* and *lw* are the action selection methods (ref. Section 4 Action selection). Interactions Approach, Shake Hands, Exchange Object are abbreviated as Appr., Sh. Hands, Exc. Obj., respectively.

Env.	Action	Appr.	Depart	Kick	Push	Sh. Hands	Hug	Exc. Obj.	Punch	Avg. AFD
FP	*bs*	.031, .02	.034, .02	.072, .04	.044, .02	.032, .01	.060, .02	.037, .05	.053, .02	.045, .01
	pe	.102, .07	.125, .10	.244, .27	.129, .10	.112, .06	.171, .11	.132, .10	.170, .11	.148, .04
	lwpe	.028, .02	.033, .02	.071, .04	.043, .02	.032, .03	.059, .03	.035, .01	.052, .02	.044, .01
	lw	.032, .02	.035, .02	.072, .04	.045, .02	.032, .02	.057, .02	.036, .02	.052, .02	.045, .01
TP	*bs*	.040, .03	.043, .03	.097, .05	.059, .03	.042, .03	.075, .04	.046, .01	.067, .03	.059, .02
	pe	.098, .04	.101, .04	.215, .08	.114, .07	.172, .07	.108, .04	.152, .04	.152, .04	.137, .04
	lwpe	.046, .04	.054, .05	.121, .06	.072, .03	.051, .03	.095, .04	.059, .02	.083, .03	.073, .02
	lw	.042, .03	.047, .03	.108, .07	.063, .03	.044, .04	.077, .04	.048, .01	.071, .03	.062, .02

Table 5: Generation accuracy (AFD) averaged over all train-test splits (mean, std. dev.) for **K3HI Interaction dataset**. *bs*, *pe*, *lwpe* and *lw* are the action selection methods (ref. Section 4 Action selection). Interactions Approach, Shake hands and Exchange object are abbreviated as Appr., Sh. Hands, Exc. Obj., respectively.

Env.	Action	Appr.	Depart	Exc. Obj.	Kick	Point	Punch	Push	Sh. Hands	Avg. AFD
FP	*bs*	.153, .99	.015, .01	.006, .01	.011, .01	.007, .00	.010, .01	.010, .00	.006, .00	.027, .05
	pe	.135, .74	.037, .03	.020, .01	.033, .02	.025, .02	.026, .02	.027, .01	.019, .02	.040, .04
	lwpe	.143, .87	.017, .02	.007, .01	.013, .01	.010, .02	.011, .01	.011, .01	.007, .01	.027, .05
	lw	.164, 1.1	.016, .01	.006, .01	.012, .01	.007, .00	.009, .01	.009, .01	.006, .00	.029, .05
TP	*bs*	.155, .96	.024, .01	.013, .01	.025, .02	.018, .02	.019, .02	.020, .01	.014, .01	.036, .05
	pe	.161, .75	.044, .02	.027, .02	.054, .03	.047, .04	.040, .02	.042, .02	.031, .02	.056, .04
	lwpe	.159, .94	.024, .02	.013, .01	.026, .02	.022, .03	.019, .01	.021, .01	.014, .01	.037, .05
	lw	.161, 1.0	.021, .02	.010, .01	.020, .01	.015, .02	.014, .01	.015, .01	.009, .01	.033, .05

Table 6: Percentage of skeleton joints (mean, std. dev.) sampled by our *pe* model from the ground truth in **first person** environment. Since *lwpe* and *lw* weigh all the skeleton joints, and *bs* observes the entire skeleton, they effectively sample 100% of the joints. Interactions Shake hands and Exchange object are abbreviated as Sh. Hands, Exc. Obj., respectively.

Dataset	Approach	Depart	Kick	Push	Sh. Hands	Exc. Obj.	Punch	Hug	Avg.
SBU	48.9, 4.2	48.7, 3.9	46.6, 2.8	49.3, 2.1	49.8, 2.3	48.9, 2.2	49.9, 3.2	48.3, 3.0	48.8, 1.0
Dataset	Approach	Depart	Exc. obj.	Kick	Point	Punch	Push	Sh. Hands	Avg.
K3HI	47.9, 3.0	47.6, 2.4	47.8, 3.0	45.8, 2.6	46.8, 4.4	47.4, 2.4	47.6, 2.0	46.3, 2.9	47.2, 1.0

Table 7: Percentage of skeleton joints (mean, std. dev.) sampled by our *pe* model from the ground truth in **third person** environment. Since *lwpe* and *lw* weigh all the skeleton joints, and *bs* observes the entire skeleton, they effectively sample 100% of the joints. Interactions Shake hands and Exchange object are abbreviated as Sh. Hands, Exc. Obj., respectively.

Dataset	Approach	Depart	Kick	Push	Sh. Hands	Exc. obj.	Punch	Hug	Avg.
SBU	47.5, 3.8	45.8, 4.6	45.1, 3.2	48.4, 2.7	47.7, 3.2	47.6, 2.8	48.7, 3.8	47.4, 2.9	47.3, 1.2
Dataset	Approach	Depart	Exc.	Kick	Point	Punch	Push	Sh. Hands	Avg.
K3HI	47.2, 2.9	47.9, 3.0	46.9, 2.9	41.1, 3.5	39.9, 7.2	45.5, 3.1	45.8, 3.7	46.8, 5.5	45.1, 3.0

Algorithm 1 The proposed agent

Initialize parameters of the generative model θ, recognition model ϕ, sequence length T.
Initialize optimizer parameters: $\beta_1 = 0.9$, $\beta_2 = 0.99$, $\eta = 0.001$, $\epsilon = 10^{-10}$.
Initialize W_0 values as 1 and $x_1^{(1:n)} \leftarrow F(X_1^{(1:n)}, W_0^{(1:n)})$, where $W_0^{(1:n)}$ are the weights for the initial sampling and the function F generates a sample $x^{(i)}$ from the environment $X^{(i)}$ after assigning weights $W_0^{(i)}$ to modality i (ref. Action selection in Section 3.3).
while true **do**
  for $\tau \leftarrow 1$ *to* T **do**
    $\hat{X}_{1:T}^{(1:n)}, \hat{y}_{1:T} \leftarrow PatternCompletion(x_{1:\tau}^{(1:n)})$
    Saliency Computation (Section 3.3 Action selection)
    $S_\tau^{(1:n)} \leftarrow g_1(X_{\tau+1}^{(1:n)}, \hat{X}_{\tau+1}^{(1:n)})$
    $W_\tau^{(1:n)} \leftarrow g_2(S_\tau^{(1:n)})$
    $x_{\tau+1}^{(1:n)} \leftarrow F(X_{\tau+1}^{(1:n)}, W_\tau)$
    Learning
    Update $\{\theta, \phi\}$ by maximizing Eq. 4.
  end for
end while

Algorithm 2 $PatternCompletion(x_{1:\tau}^{(1:n)})$

for $t \leftarrow 1$ *to* T **do**
  Recognition Model
  for $i \leftarrow 1$ *to* n **do**
    if $t > \tau$ **then**
      $x_t^{(i)} \leftarrow \hat{X}_t^{(i)}$
    end if
    $[\mu_{0,t}^{(i)}; \sigma_{0,t}^{(i)}] \leftarrow \varphi^{prior}(h_{t-1}^{(i)})$
    $[\mu_{z,t}^{(i)}; \sigma_{z,t}^{(i)}] \leftarrow \varphi^{enc}([x_t^{(i)}, h_{t-1}^{(i)}])$
  end for
  Product of Experts
  $z_t \sim \mathcal{N}(\mu_{\mathbf{0},\mathbf{t}}, \mathbf{diag}(\sigma_{\mathbf{0},\mathbf{t}}^{\mathbf{2}}))$, where $\sigma_{\mathbf{0},\mathbf{t}}^{\mathbf{2}} = \Big(\sum_{i=1}^{n} (\sigma_{0,t}^{(i)})^{-2}\Big)^{-1}$ and $\mu_{\mathbf{0},\mathbf{t}} = \Big(\sum_{i=1}^{n} \mu_{0,t}^{(i)} (\sigma_{0,t}^{(i)})^{-2}\Big)\sigma_{\mathbf{0},\mathbf{t}}^{\mathbf{2}}$
  $z_t|\mathbf{x}_t \sim \mathcal{N}(\mu_{\mathbf{z},\mathbf{t}}, \mathbf{diag}(\sigma_{\mathbf{z},\mathbf{t}}^{\mathbf{2}}))$, where $\sigma_{\mathbf{z},\mathbf{t}}^{\mathbf{2}} = \Big(\sum_{i=1}^{n} (\sigma_{z,t}^{(i)})^{-2}\Big)^{-1}$ and $\mu_{\mathbf{z},\mathbf{t}} = \Big(\sum_{i=1}^{n} \mu_{z,t}^{(i)} (\sigma_{z,t}^{(i)})^{-2}\Big)\sigma_{\mathbf{z},\mathbf{t}}^{\mathbf{2}}$
  Generative Model
  for $i = 1$ *to* n **do**
    $h_t^{(i)} \leftarrow RNN_\theta(h_{t-1}^{(i)}, [z_t, x_t^{(i)}])$
    $[\mu_{x^{(i)},t}^{(i)}; \sigma_{x^{(i)},t}^{(i)}] \leftarrow \varphi^{dec}([h_{t-1}^{(i)}, z_t])$
    $\hat{X}_t^{(i)} \leftarrow \mu_{x^{(i)},t}^{(i)}$
  end for
  Classification Model
  $h_t^{(n+1)} \leftarrow RNN_\theta(h_{t-1}^{(n+1)}, [z_t, \mathbf{x}_t, h_t^{(1:n)}])$
  $\hat{y}_t \leftarrow softmax([h_{t-1}^{(n+1)}, z_t])$
end for

S.3.2 Examples of interaction generation by our model

See Figs. 5, 6, 7, 8.

S.4 Discussion

S.4.1 Handling missing class labels

Our model requires true class labels to train for classification. A subset of parameters is shared between the classification and generation pathways. The generation and class label are independent outputs.

When class labels are missing, the generative parameters, including the shared parameters, are trained to minimize the generative loss only. The model continues to infer irrespective of whether labels are present, noisy or missing, which makes it practical for real-world applications. Since the generation and classification pathways share parameters, even if the class labels are missing, the shared parameters will be updated by minimizing the generative error only which might improve the classification accuracy.

S.4.2 Number of trainable parameters

Number of trainable parameters for all model variants is shown in Table 8. TP variants have less trainable parameters than FP. *lwpe* and *lw* have more parameters than *pe* or *bs*.

Table 8: Number of trainable parameters.

Action	FP	TP
bs	1656348	1089996
pe	1656348	1089996
lwpe	1657728	1092726
lw	1657728	1092726

S.4.3 Training time

Our model is implemented using TensorFlow 1.3 framework in Python 3.5.4. All experiments are carried out in HPC using PowerEdge R740 GPU nodes equipped with Tesla V100-PCIE-16GB.

Training time is the total time required for training the model on the trained set until the error converges. The training time for our models is shown in Table 9. We report the average (over n-fold cross validation) convergence time in hours and the average number of iterations in Table 9. In order to identify offline the iteration at which convergence occurs, we smooth the classification accuracy and the generation error curves by calculating the moving average with a 50-iteration window. For classification, we consider convergence is reached at the iteration when the average accuracy exceeds 90% of the highest accuracy.

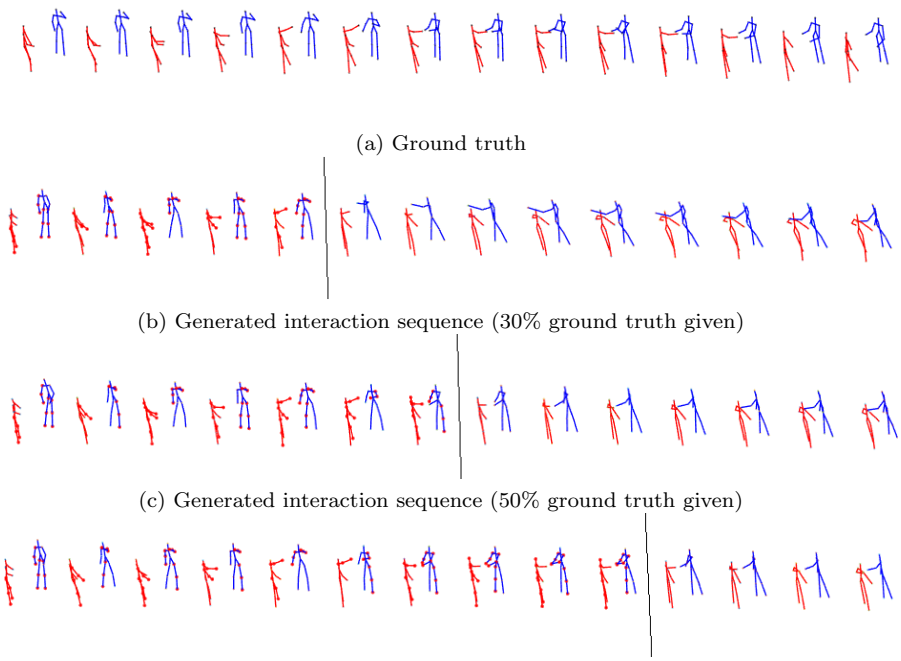

(a) Ground truth

(b) Generated interaction sequence (30% ground truth given)

(c) Generated interaction sequence (50% ground truth given)

(d) Generated interaction sequence (70% ground truth given)

Figure 5: Interaction generation in **first person for exchanging object in SBU dataset**. The top (or first) row shows the true skeletal data. Each skeleton in second, third and fourth rows is one step ahead prediction until 30%, 50% and 70% of the ground truth respectively (demarcated by the black vertical line). Beyond that, the model uses its own prediction as input for completing the interactions until the final time step. At each given time step, the salient joints are marked red. Every other time step is shown.

Table 9: Training time (in hours), number of iterations.

Action Selection	SBU		K3HI	
	FP	TP	FP	TP
bs	1.0, 7368	0.4, 4364	1.6, 5388	0.7, 2452
pe	1.8, 7146	0.5, 4166	5.2, 9154	1.8, 7199
lwpe	1.2, 5512	0.5, 2844	2.7, 5421	2.5, 5832
lw	1.4, 5203	1.3, 6889	4.6, 10519	2.0, 3350

S.4.4 End-to-end training

End-to-end training allows an entire model to be optimized for a given task(s) and dataset. However, the challenge is to search for the optimal set of parameter values in a very large space. This is often circumvented by *pretraining* selected components (layers, blocks, functions) in isolation for a number of iterations to initialize their parameters in a sub-optimal space. Then the entire model is trained end-to-end. Our model is trained end-to-end, without any pretraining.

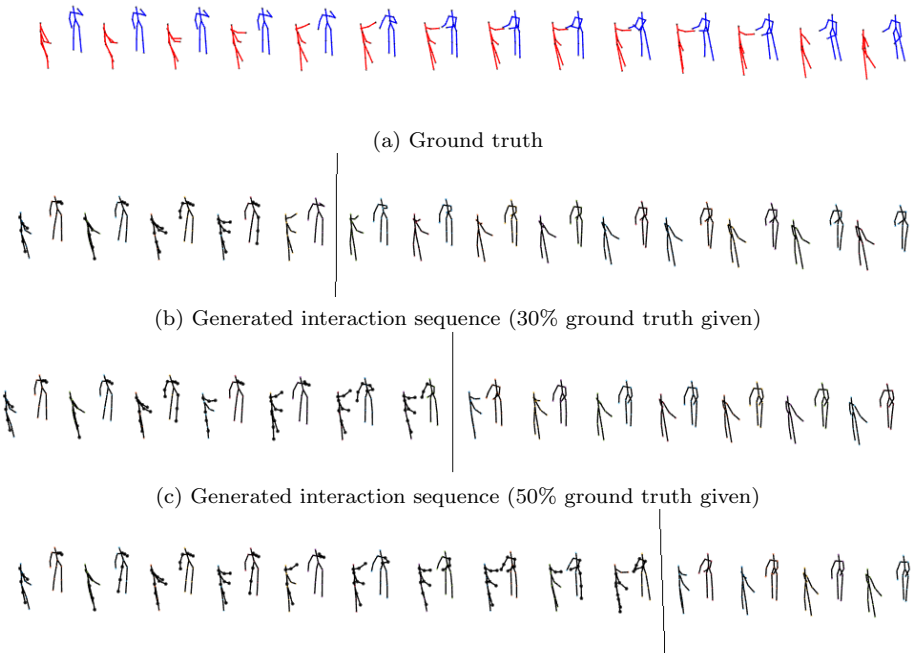

(a) Ground truth

(b) Generated interaction sequence (30% ground truth given)

(c) Generated interaction sequence (50% ground truth given)

(d) Generated interaction sequence (70% ground truth given)

Figure 6: Interaction generation in **third person for exchanging object in SBU dataset**. The top (or first) row shows the true skeletal data. Each skeleton in second, third and fourth rows is one step ahead prediction until 30%, 50% and 70% of the ground truth respectively (demarcated by the black vertical line). Beyond that, the model uses its own prediction as input for completing the interactions until the final time step. At each given time step, the salient joints are marked black. Every other time step is shown.

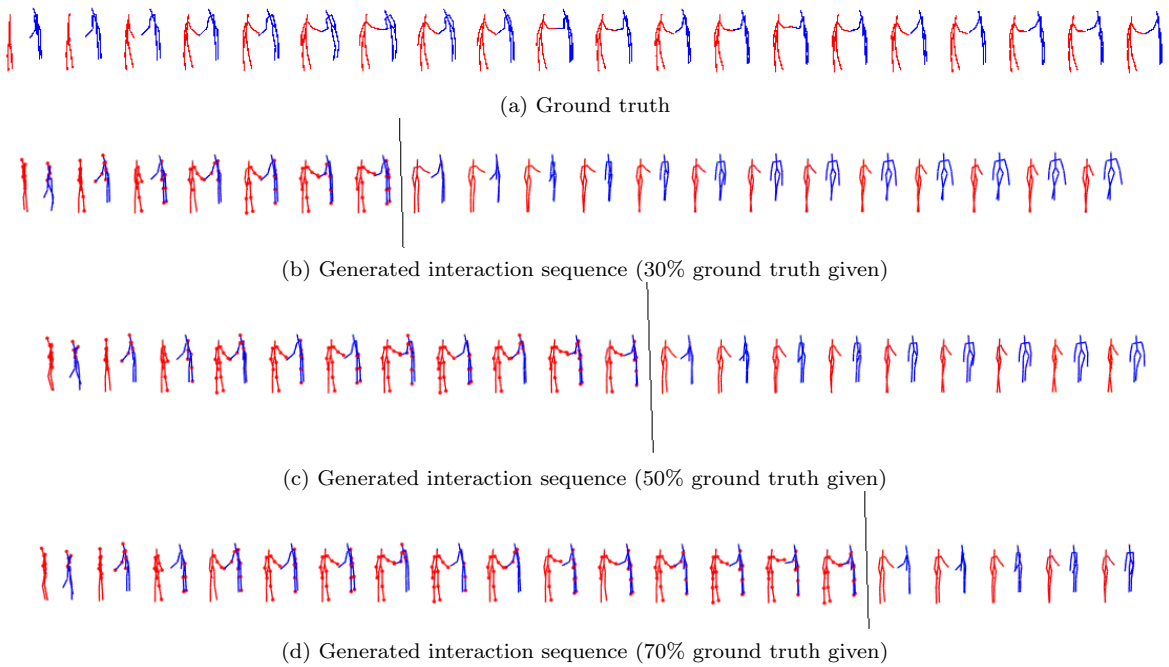

(a) Ground truth

(b) Generated interaction sequence (30% ground truth given)

(c) Generated interaction sequence (50% ground truth given)

(d) Generated interaction sequence (70% ground truth given)

Figure 7: Interaction generation in **first person for shaking hands in K3HI dataset**. The top (or first) row shows the true skeletal data. Each skeleton in second, third and fourth rows is one step ahead prediction until 30%, 50% and 70% of the ground truth respectively (demarcated by the black vertical line). Beyond that, the model uses its own prediction as input for completing the interactions until the final time step. At each given time step, the salient joints are marked red. Every third time step is shown.

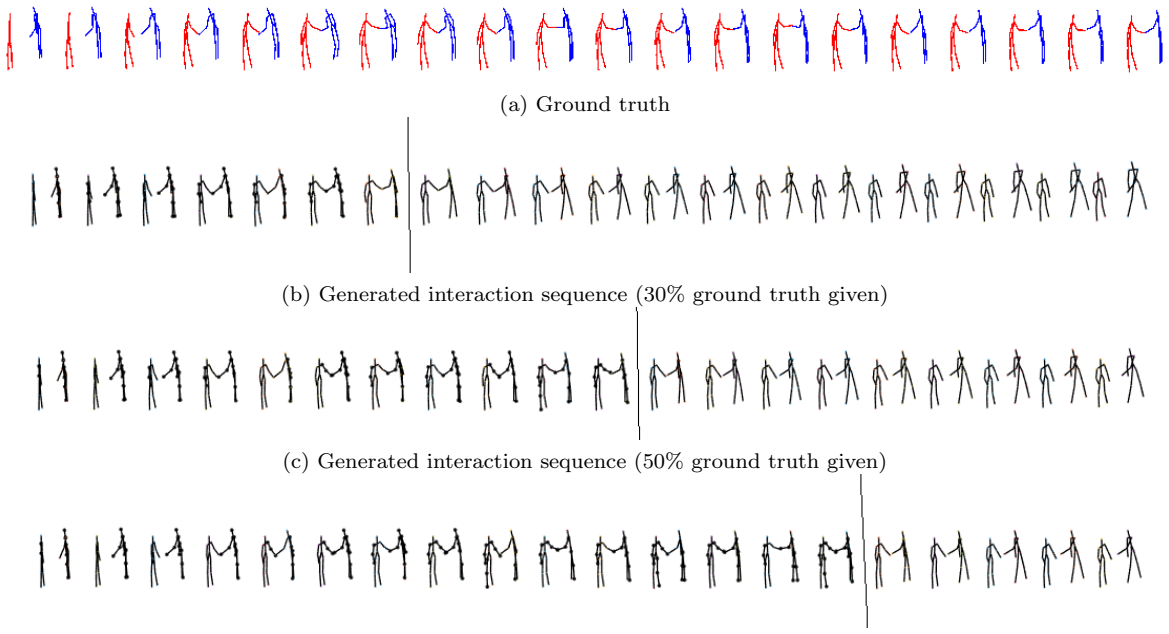

(a) Ground truth

(b) Generated interaction sequence (30% ground truth given)

(c) Generated interaction sequence (50% ground truth given)

(d) Generated interaction sequence (70% ground truth given)

Figure 8: Interaction generation in **third person for shaking hands in K3HI dataset**. The top (or first) row shows the true skeletal data. Each skeleton in second, third and fourth rows is one step ahead prediction until 30%, 50% and 70% of the ground truth respectively (demarcated by the black vertical line). Beyond that, the model uses its own prediction as input for completing the interactions until the final time step. At each given time step, the salient joints are marked black. Every third time step is shown.